Realistic Design Studies on a 300-GHz, 1-MW, DEMO-Class Conventional-Cavity Gyrotron

Debasish Mondal, S. Yuvaraj, Meenakshi Rawat, M. K. A. Thumm, *Life Fellow, IEEE* , and M. V. Kartikeyan, *Fellow, IEEE*

***Abstract* — This paper presents realistic initial design studies of a 300 GHz, 1 MW, conventional cavity gyrotron for its probable application in the next generation thermonuclear fusion reactors. Keeping the design goals, parameters and constraints in view, the very high-order $TE_{49,18}$ mode is chosen as the operating mode after a careful mode selection calculation considering realistic ohmic cavity losses. After mode selection and mode competition studies, the cold cavity design and initial design of a triode-type magnetron injection gun (T-MIG) and a gyrotron magnet are carried out and an electron beam radius of 8.11 mm is obtained with 2.4 % velocity spread. Further investigation on RF behavior of the cavity is performed with the T-MIG beam parameters. By varying the nominal beam parameters, single-mode self-consistent calculations are conducted and achieved the desired output power with efficiency > 31 %. Then, multi-mode time-dependent self-consistent calculations are carried out before and after space-charge neutralization with beam radius spread and realistic velocity spread for the assessment of the start-up scenario. Before space-charge neutralization, the beam voltage is depressed to 70.08 kV and 0.72 MW output power is obtained, whereas after 60 % of space-charge neutralization in the start-up scenario, the beam voltage increases to 74.83 kV and thereby an output power of 0.92 MW is obtained with 8.11 mm of beam radius.**

***Index Terms*— Conventional cavity gyrotron, DEMO tokamak, electron cyclotron resonance heating (ECRH), space-charge neutralization, triode magnetron injection gun (T-MIG).**

I. Introduction

GYROTRONS are the most capable and powerful coherent sources to generate very high output power (MW) in sub-millimeter wave ranges. In the high-frequency regime (100 - 300 GHz), the potential applications of high-power gyrotrons (> 1 MW) are Electron Cyclotron Resonance Heating (ECRH), non-inductive Current Drive (CD) of plasmas, plasma start-up, and plasma stability control in fusion research [1]–[4]. Recently, a significant effort has been done for the installation of the first batch of 24 Continuous Wave (CW) gyrotrons to generate 24 MW RF power where each gyrotrons can

Debasish Mondal, Meenakshi Rawat and M. V. Kartikeyan are with the Department of Electronics and Communication Engineering, Indian Institute of Technology Roorkee, Roorkee 247667, India. Presently, M. V. Kartikeyan is on deputation with the Department of Electrical Engineering, Indian Institute of Technology, Tirupati, Andhra Pradesh, 517506, India. (E-mail: dmondal@ieee.org; kartik@ieee.org)

S. Yuvaraj is with the Department of Electronics and Communication Engineering, National Institute of Technology Andhra Pradesh, India.

M. K. A. Thumm is with the Karlsruhe Institute of Technology, Insti- tute for Pulsed Power and Microwave Technology, D-76344 Karlsruhe, Germany.

deliver 1 MW power at 170 GHz to support plasma heating in the International Thermonuclear Experimental Reactor (ITER) tokamak in Cadarache, France [5], [6]. The physical designing and testing of high-power gyrotrons at different reactors for controlled fusion (CF) have confirmed their ECRH heating capability. After ITER, the recent development of the first prototype of a commercial fusion reactor, the DEMOnstra- tion (DEMO) tokamak has boosted the interest of different research groups worldwide. However, the DEMO gyrotron (successor of ITER tokamak gyrotron) requires careful study to meet the challenges of generating high-power in the high- frequency regime (above 200 GHz). Different research groups are already involved in meeting these challenges. For exam- ple, Fusion Long Pulse Gyrotron Laboratory (FULGOR) at Karlsruhe Institute of Technology (KIT) has made an effort to develop an in-house testing facility for the characterization of high-power gyrotrons for DEMO [7], [8]. Similarly, the EUROfusion Heating and Current Drive work package (WP HCD) is involved in the development of megawatt-class CW gyrotrons (conventional and coaxial) at 240 GHz [9], whereas a preliminary feasibility analysis of a 0.24 THz coaxial cavity gyrotron has been carried out to achieve 2 MW of output power in [10]. Notably, the experimental operation of a 250 GHz gyrotron has been reported with the output power of 330 kW in [11]. A 203 GHz gyrotron has been developed with high interaction efficiency, and collaborative work is in progress at Plasma Research Center (PRC) at the University of Tsukuba with National Institutes for Quantum and Radiological Science and Technology (QST) to develop a 300 GHz gyrotron to support ECCD and ECRH on DEMO tokamak with high output RF power [12]. The initial design studies on the DEMO tokamak reported that a high CD efficiency could be achieved using RF power at optimum frequencies in two scenarios, one for steady-state operation around 230 GHz and another for pulsed operation around 290 GHz [13]. The targeted output power of the DEMO gyrotrons should be larger than 1 MW at frequencies above 200 GHz with > 95 % Gaussian output beam [14]. A systematic design study of DEMO gyrotrons with an output power of 1-2 MW operating at 200 GHz has been reported by Thumm *et al.* [14]. The realistic assesment on the operation of a 236 GHz hollow cavity gyrotron have been carried out in [15] and the effect of thermoanalysis on operation of a 240 GHz gyrotron has been reported in [16]. The validation of the stable operation with the desired output power (3 MW), including the space-charge neutralization effect, has been carried out by our research group for the multifrequency

TABLE I
DESIGN GOALS AND CONSTRAINTS

Frequency (f_r)	300 GHz
Output Power (P_{out})	≈ 1-2 MW
Diffractive Quality Factor of Cavity (Q_d)	≈1250-1350
Electron Beam Voltage (V_b)	70-81 kV
Electron Beam Current (I_b)	36-48 A
Magnetic Field at Cavity Center (B_0)	9-12 T
Total Output Efficiency (η_{total})	≥ 30 %
Estimated Cavity Wall Losses (ρ_0)	< 2 kW/cm^2
Total Losses	<8 %

DEMO gyrotron [17].

In the present work, a first-cut design study of a DEMO class conventional cavity gyrotron has been presented. The study includes mode-selection calculations, design of triode magnetron injection gun (T-MIG), cold cavity design and studies on RF behavioral aspects. From the literature, it is evident that the conventional cavity gyrotron is extensively used in ECRH and ECCD systems (tokamak: ITER, ASDEX-Upgrade, DIII-D, EAST, KSTAR, stellarator: W7-X) due to its simple design and stable output operation [9]. The principal frequency of 300 GHz is selected in this work to match the compatibility of the DEMO class gyrotron for the application in the ECRH system. Further, by considering the guidelines of EU-DEMO1-2015 for DEMO tokamak, the output RF power is targeted at 1 MW to reduce the number of gyrotrons in tandem and hence relax the maintenance requirements of the tokamak [9]. The primary design goals and technical constraints are given in Table I.

Organization of the paper is as follows: In section II, the mode selection calculation, cold-cavity design, and single-mode self-consistent calculations are performed and presented using our in-house code Gyrotron Design Suite (GDS-2018) [18], while a design methodology of T-MIG using the commercial tool EGUN [19] is presented in section III. In section IV, the beam parameters obtained from the designed electron gun are further employed to perform the time-dependent self-consistent calculations before and after space-charge neutralization using the KIT SELFT code [20] and finally, in Section V, the significant findings of the work are highlighted pointing out the scope for further work.

II. MODE SELECTION AND CAVITY DESIGN

The operation of the DEMO gyrotrons, at a very high-frequency 300 GHz with high output power > 1 MW, requires a larger cavity radius to mitigate the wall-loading effects. The eigenvalue of more than 120 allows the gyrotron to have a larger cavity radius and significantly better power handling capability. However, this also increases the density in the mode spectrum and invites higher mode competition. So, it is a very tedious process to excite the desired cavity mode in a dense mode spectrum. Hence, DEMO gyrotrons require a precise cavity design with optimized operating parameters for the steady operation with the chosen mode. The cavity radius R_0 is related to the eigenvalue $\chi_{m,p}$ of the $\mathrm{TE}_{m,p}$ mode by

TABLE II
PROBABLE CAVITY MODES CONSIDERED FOR THE DESIGN OF DEMO CLASS GYROTRON

m	p	χ_{mp}	R_0 (mm)	R_b (mm)	I_L (A)	$(\chi^2_{m,p} - m^2)$	$m_2/2$
46	19	120.7112	19.21	7.62	59.6	12455.2	2.66
47	19	121.986	19.41	7.79	60.3	12671.6	2.67
48	19	123.2584	19.62	7.95	61.0	12888.6	2.68
49	**18**	**121.102**	**19.27**	**8.11**	**63.7**	**12264.7**	**2.72**
49	19	124.5284	19.82	8.11	61.7	13106.3	2.69
50	18	122.3631	19.47	8.27	64.4	12472.7	2.73
50	19	125.7959	20.02	8.27	62.4	13324.6	2.70
51	17	120.1626	19.12	8.43	67.3	11838.0	2.77
51	18	123.6218	19.68	8.43	65.1	12681.3	2.74
51	19	127.0612	20.22	8.43	63.1	13543.5	2.71
52	17	121.4122	19.32	8.60	68.1	12036.9	2.78
52	18	124.8782	19.87	8.60	65.8	12890.6	2.75
52	19	128.3241	20.42	8.60	63.7	13763.1	2.72
53	17	122.6597	19.52	8.76	68.8	12236.4	2.80
53	18	126.1325	20.07	8.76	66.5	13100.4	2.76
53	19	129.5849	20.62	8.76	64.4	13983.2	2.73

$R_0 = \chi_{m,p}\lambda/2\pi$, where the free-space wavelength is denoted by λ. The optimum value of the electron beam radius R_b for the first beam harmonic ($s = 1$) operation is calculated using $R_b = \chi_{m\pm1,i}R_0/\chi_{m,p} = \chi_{m\pm1,i}\lambda/2\pi$, where i is the radial field maximum [2]. Table II contains probable modes along with design constraints considered for the current design of 1 MW gyrotron operating at 300 GHz. These modes offer a larger cavity radius in order to control the ohmic wall loading at 300 GHz. As a matter of experience the modes with mode eigenvalues between 120-130 are considered for the present case and design constraints are computed following standard analytical expressions with Gaussian beam approximation [2] (see Table II).

An important criteria for mode selection is that the candidate mode should support an advanced dimpled wall launcher for radial extraction of the power output. For this, the factor $m_2/2 = \pi/\cos^{-1}(m/\chi_{m,p})$, which gives the number of reflections on the output waveguide wall per turn has been computed. Though it is not mandatory, it is desirable to have $m_2/2 \approx 3.0$ for a single-beam output scheme and ≈ 2.5 for a dual-beam output scheme. As a matter of practice, $m_2/2 \approx 2.6 - 3.1$ are considered for mode selection here. We have computed cavity radius R_0, beam radius R_b, voltage depression V_d, limiting current I_L, wall-loading factor $(\chi^2_{m,} - m^2)$ and $m_2/2$. For a given mode, the position of electron beam is fixed close to the first radial electrical field maximum to achieve maximum coupling between the electromagnetic field and the electron beam. V_d of the electron beam depends on the position of the electron beam with respect to R_0. The V_d is inversely proportional to I_L. The lower V_d is, the higher I_L can be achieved and hence the device can be operated at higher electron beam current (I_b). The wall loading is denoted as $\frac{dP_{loss}}{dA} \simeq \left(\frac{\delta}{4\pi\mu_0\omega}\right)\frac{1}{(\chi^2_{m,p} - m^2)}\left(k_m^4 \left|J_{m-1}(\chi_{m,p})\right|^2 + \frac{m^2}{R^2}\left|\frac{dV_{mp}}{dz}\right|^2\right)$. The acceptable level of ohmic wall loading for the available cooling system is 2.5 kW/cm^2, when Glidcop is used as the interaction cavity material [3]. In the present design of the 300 GHz gyrotron, the tolerance limit is set to 2 kW/cm^2, so that the proposed design can support the practical development even with the use of the ordinary copper material. If the tolerance

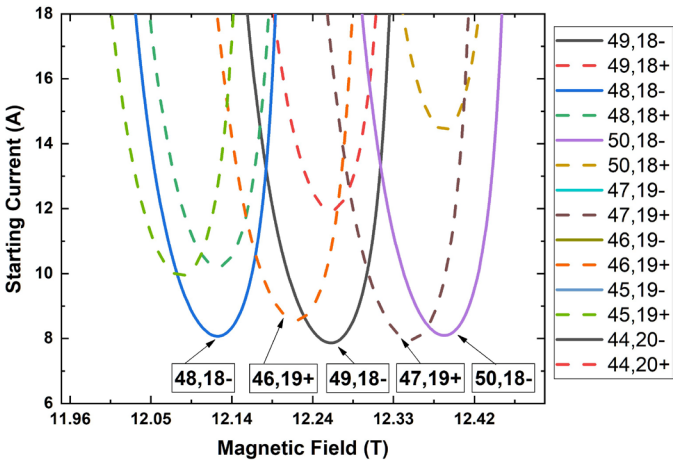

Fig. 1. Starting current as a function of magnetic field for the de- sired mode **TE49,18** along with the major competing modes for the beam parameters α = 1.3, V_b = 78 kV, R_0 = 19.27 mm, R_b = 8.11 mm, Q_d = 1305.

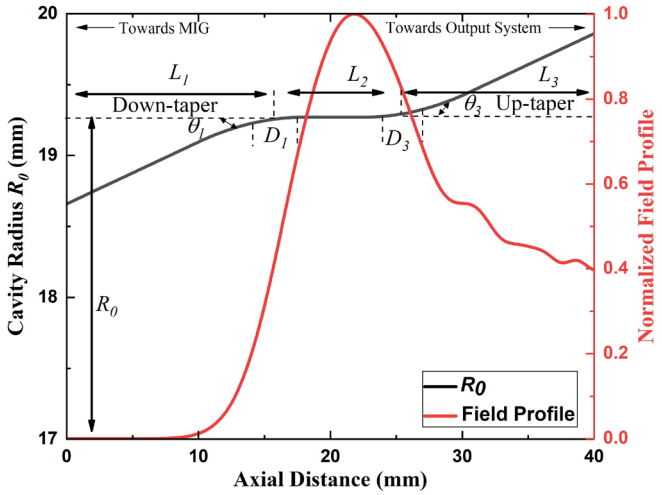

Fig. 2. Distribution of amplitude of electric field in the cavity at its resonant frequency, normalized with respect to its corresponding value at its center, obtained by using GDS-2018 [18].

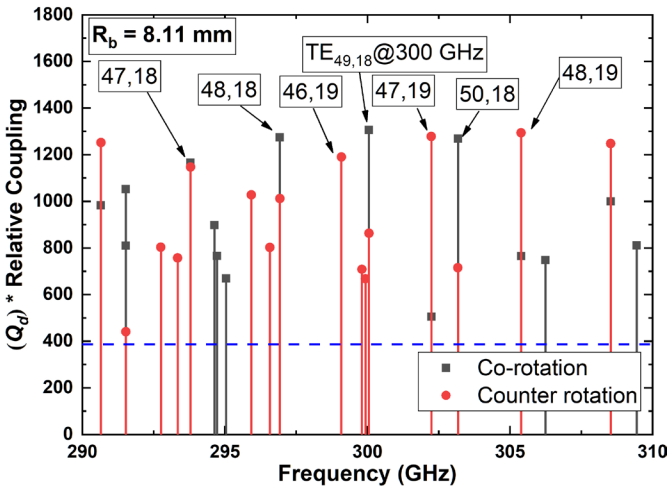

(a)

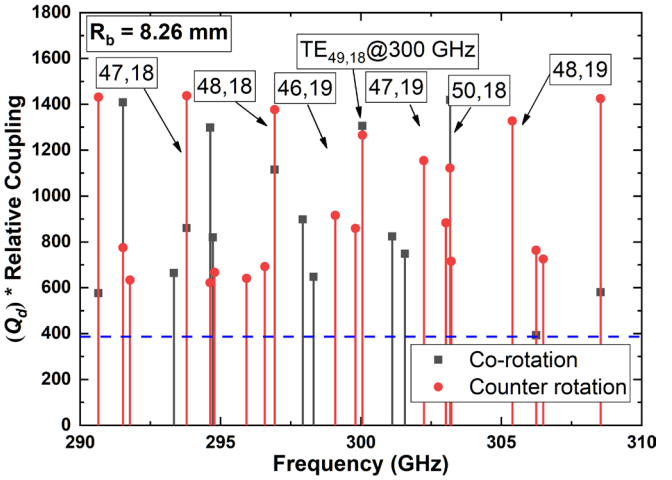

(b)

Fig. 3. Diffractive quality factor (Q_d) times relative coupling co-efficient of the desired mode along with other competing modes, obtained using GDS-2018 [18] with the beam radius of R_b = 8.11 and 8.26 mm in the frequency range 290 to 310 GHz.

level in the present design is increased to 2.5 kW/cm^2, the chosen cavity mode of the proposed gyrotron can support the slightly higher power operation than 1 MW. A detailed study of strategic mode selection for high power gyrotrons has been reported by Franck *et al.* [21]. By satisfying all these technical constraints and based on our design goals as stated in Table I, the mode TE$_{49,18}$ is finalized as the operating mode for this design. Further, the starting current calculations are performed to estimate the separation between the TE$_{49,18}$ mode with the major competing modes operating with the same beam radius. Fig. 1 shows the co-rotating modes TE$_{48,18}$ and TE$_{50,18}$ are well separated from main mode.

After the selection of the suitable mode, cold cavity calculations and self-consistent single-mode calculations are carried out using GDS-2018 [18] by solving the equation of parti- cles with single-mode Vlasov's equation through leap frog algorithm by considering the following approximations: (a) mode coupling is ignored, (b) RF field is assumed to be constant during the transit of electron beam, and (c) external magnetic field is considered along the direction of wave propagation. The design of the conventional-cavity interaction structure is carried out through cold cavity calculations. The cylindrical interaction structure comprises an input down-taper section L_1, a straight mid-section L_2, and an up-taper section L_3, as shown in Fig. 2. The up-taper section L_3 is further connected to the output system through nonlinear taper for the maximum transmission of the RF fields, whereas the input down-taper section L_1 ensures the blocking of the reflected RF waves propagating towards the T-MIG. Moreover, the tapering of the input and output cavity sections ensures a significantly high-quality factor and better field profile inside the interaction cavity. Also, parabolic roundings D_1 and D_3, along with the tapering angles θ_1 and θ_3, reduce unwanted mode conversion due to sharp transitions in the input and output taper sections. The mid-section length predominantly determines the diffractive quality factor (Q_d) of the cavity. So, an increase in the Q_d increases the interaction efficiency;

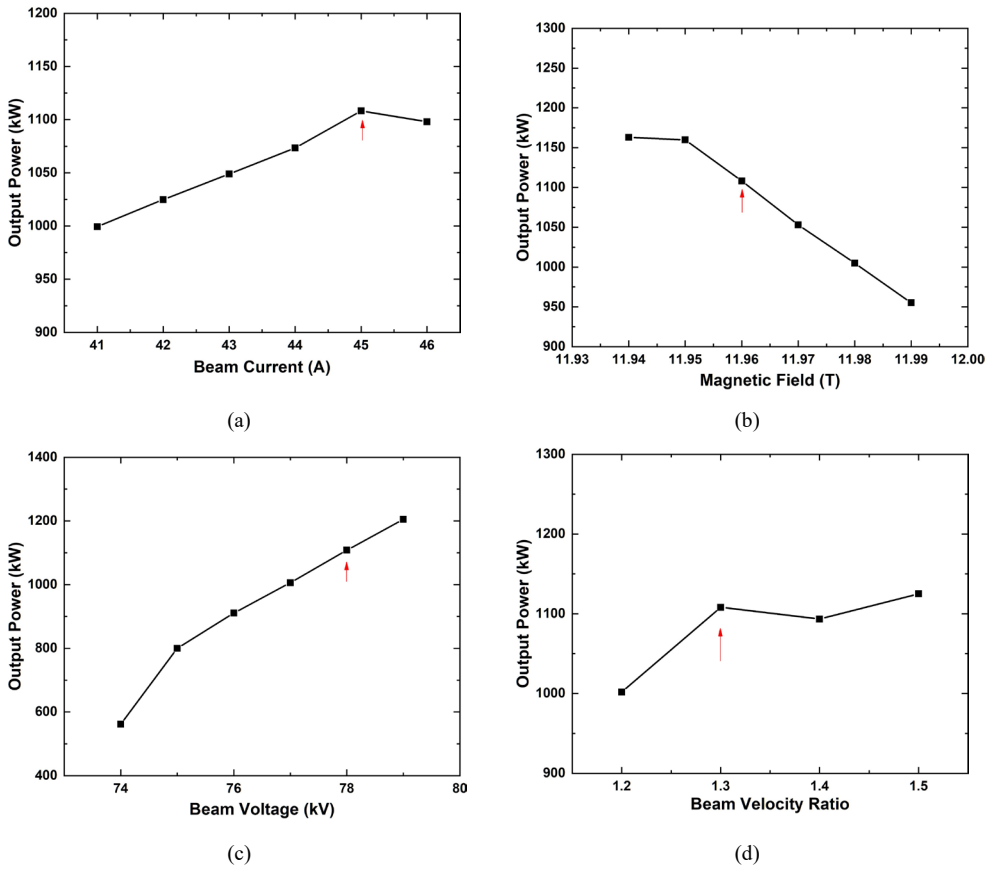

Fig. 4. Output power as a function of (a) beam current with V_b = 78 kV, B_0 = 11.96 T, and α = 1.3, (b) magnetic field with I_b = 45 A, V_b = 78 kV, and α = 1.3, (c) beam voltage with I_b = 45 A, B_0 = 11.96 T, and α = 1.3,and (d) beam velocity ratio with I_b = 45 A, V_b = 78 kV, and B_0 = 11.96 T.

however, it also increases the ohmic Q-factor (Q_Ω) and results in a rise in the ohmic wall loading. The relation between Q_d and Q_Ω can be expressed as, $\frac{1}{Q} = \frac{1}{Q_d} + \frac{1}{Q_\Omega}$, where Q is the total quality factor. Hence, a trade-off is required between the interaction efficiency and the ohmic wall loading. Since the $TE_{49,18}$ mode operates near its cut-off frequency, the radius of the interaction cavity midsection is R_0 = 19.27 mm for maximum coupling between the RF wave and the annular electron beam and the longitudinal dimensions of the interaction cavity L_2 = 12.5 mm, $L_1 = L_3$ = 14 mm, and taper angles $\theta_1 = \theta_3$ = 2.5 ° are chosen to give a Q_d 1300. The optimized parameters of the cavity geometry along with the normalized electric field profile are shown in Fig. 2, and the interaction cavity dimensions are listed in Table III.

After cold cavity computations, to understand the mode-competition, the beam-coupling coefficient is deter- mined for the modes with the resonant frequency be- tween 290-310 GHz for the beam radius R_b of 8.11 and 8.26 mm. The coupling co-efficient is denoted as, $G_{m,p} = J_{m\pm1}(k_{\perp m,p}R_b)/J_m(\chi_{m,p})\ \pi\ \chi^2_{m,}\ m^2$, where $k_{\perp m,p}$ is the perpendicular wave number and J_m is the Bessel func- tion [2]. The coupling coefficients (CC) of the neighboring modes are normalized with respect to the desired mode. In Fig. 3, Q_d times relative CC values are calculated for neigh- boring modes along with the main mode at their respective resonant frequencies in the designed interaction cavity with the beam radius of 8.11 and 8.26 mm. The modes with $Q_d * CC$ value greater than 30% of that of the desired mode offer severe mode competition. In Fig. 3, the threshold line is set around 391 (30% of Q_d CC value of the main mode) and marked in the blue line. From Fig. 3(a), it can be noted that the major competing modes for the chosen cavity mode $TE_{49,18-}$ are $TE_{48,18-}$, $TE_{50,18-}$, $TE_{46,19+}$, and $TE_{47,19+}$. These competing modes are fairly separated from the desired frequency of 300 GHz. Also, it is observed in Fig. 3(b) that the relative coupling of the immediate nearby counter-rotating modes $TE_{46,19}$, and $TE_{47,19}$ decreases, whereas the relative coupling of other nearby counter-rotating modes $TE_{48,18}$, $TE_{48,19}$ increases with the increase of the beam radius from 8.11 to 8.26 mm. In turn, the beam-coupling coefficients of the $TE_{48,19}$ co-rotating and counter-rotating modes are equal for the beam radius of 8.26 mm and this restricts the possible upper beam radius choice. These results indicate that mode competition is not changed significantly with the change in the beam radius.

In the next step, single-mode self-consistent calculations are carried out by varying the nominal beam and magnetic field parameters (V_b, I_b, α, B_0) to calculate optimal values for the desired output power of 1 MW with maximum efficiency. The graphical presentation of the parametric analysis is shown in Fig. 4. The working ranges of beam parameters are I_b = 41- 46 A, B_0 = 11.94-11.99 T, V_b = 74-79 kV, and α = 1.2-1.5 re-

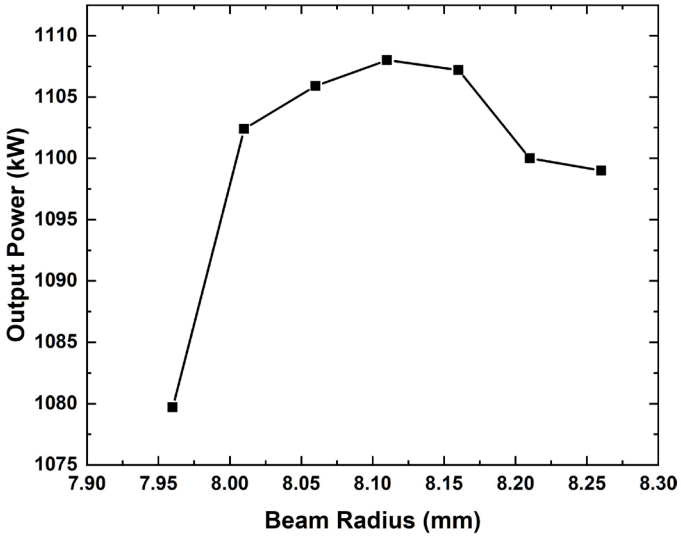

Fig. 5. Effect of beam radius (R_b) on the output power on a 300 GHz gyrotron operation

TABLE III
OPTIMIZED CAVITY GEOMETRY WITH SINGLE MODE RESULTS OBTAINED USING GDS-2018 [18]

Parameters	Values
$L_1/L_2/L_3$	14/12.5/14 mm
θ_1/θ_3	2.5/2.5 °
D_1/D_3	4/4 mm
R_0	19.27 mm
Q_d	1305
f_r	300.005 GHz
R_b	8.11 mm
V_b	78 kV
I_b	45 A
B_0	11.96 T
a	1.3
P_{out}	1108 kW
ρ_0	1.91 kW/cm^2
η_{total} (*incl.*ρ_0)	31.59 %

[*resonant frequency f_r, beam voltage V_b, beam current I_b, magnetic field B_0, output power P_{out}, wall-loading ρ_0, total efficiency including wall losses η_{total}]

spectively. The optimized operating points are marked in red arrow in Fig. 4. Additionally, the effect of beam radius (R_b) deviation on the output power is presented in Fig. 5. The output power decreases with the variation of R_b from its optimum value due to the reduction in the beam coupling. It is evident from Fig. 3 and Fig. 5 that a beam radius of 8.11 mm provides better stability and coupling. The geometrical dimensions of the interaction cavity along with self-consistent single mode results for optimized set of nominal parameters are given in Table III. The conductivity of the cavity material (Glidcop) changes due to the surface roughness (h) and enhancement of temperature (T_C) from 5.7×10^7 S/m to its effective value $\sigma_{\text{Glidcop,eff}}$ [22]. Using GDS-2018 [18], the value of $\sigma_{\text{Glidcop,eff}}$ is determined as 1.75×10^7 S/m and is used in the self-consistent calculations.

TABLE IV
MAGNETIC FIELD REQUIREMENT ALONG THE GYROTRON GEOMETRY

Descriptions	Values
Peak magnetic field at cavity center (Z_C)	B_0 = 11.96 T
Magnetic field deviation at -5 mm ≤ Z_C ≤ +5 mm	$\lvert\Delta B\rvert \le 0.001\ B_0$
Magnetic field strength (B_E) at MIG	$0.02\ B_0 \le B_E \le 0.05 B_0$
Minimum magnetic field (B) at output side	$B \ge 0.12 B_0$

TABLE V
OPTIMIZED COIL DATA OBTAINED USING GDS-2018 [18]

Coils	Width ΔZ (mm)	Height ΔR (mm)	Coil Radius R_C (mm)	Winding Turns N_C	Current (A)
Main Coil-1	400	15	100	27429	149
Main Coil-2	100	15	115	1250	149
Main Coil-3	100	15	115	1250	149
Gun Coil	41	15	100	1167	-89

III. DESIGN STUDIES OF TRIODE-TYPE MAGNETRON INJECTION GUN

The magnetron injection gun (MIG) is a crucial component of gyrotrons to generate the gyrating annular electron beam. After being extracted from the cathode emitting strip, the electron beam gyrates under the influence of the magnetic field. The electron beam parameters are the pivotal element for the interaction between the transverse RF electric field and the electron beam for efficient power transfer from the electron beam to RF waves. In the present design, we have considered a triode-type magnetron injection gun (T-MIG) as it gives more flexibility in controlling beam parameters. From the calculations performed in Section-II, we have a basic idea of the cavity radius, beam radius, magnetic field at the emitter position and at the cavity mid-section.

The gyrotron interaction cavity is surrounded by the superconducting magnet (SCM), where the midsection (L_2) has the maximum magnetic field and decreases significantly on both sides of the interaction cavity in order to avoid unwanted before and after cavity interactions [23]. The minimum bore-hole diameter of the SCM depends on the maximum beam diameter of the T-MIG. According to Busch's theorem, the electron beam radius (R_b) and cathode radius (R_c) is related by $R_c = bR_b$, where the compression ratio $b = B_0/B_E$ [2]. In this work, four solenoid coils are used to generate the required magnetic field profile. For employing more realistic design approach of magnetic guidance system, one main coil with two auxiliary coils are placed at the center position to produce the static magnetic field along the interaction cavity, and a gun coil is aligned at the emitter region. The gun coil provides the flexibility to control the strength of the magnetic field at the emitter region. The minimum design requirements of the magnetic field are stated in Table IV, where the magnetic coils data for achieving the desired field profile are provided in Table V. The achieved magnetic field profile further employed in the EGUN simulation is shown in Fig. 6.

The primary objective behind the optimization process of T-MIG and the magnetic guidance system is to generate a high-quality annular electron beam with low electron velocity

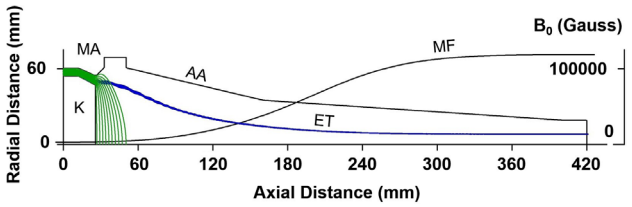

Fig. 6. Optimized electron beam trajectory along the gyrotron axial length obtained using EGUN [19]. (K: cathode; MA: modulating anode; AA: accelerating anode; ET: electron trajectory; MF: magnetic field).

TABLE VI
GEOMETRICAL PARAMETERS AND SIMULATED RESULTS OF T-MIG

Parameters	Values
Accelerating Voltage (V_{acc})	78 kV
Modulating Anode Voltage (V_{mod})	35.5 kV
Cathode Radius (R_c)	51 mm
Cathode Angle	28 °
Anode Radius (R_a)	62 mm
Electron Beam Current (I_b)	45 A
Emitter Current Density (J_e)	3 A/cm^2
Modulating Anode Angle	25 °
Slant Length (L_e)	4.12 mm
Spacing between Cathode and Mod. Anode	5.5 mm
Results	
Magnetic Field at Emitter Region (B_E)	0.210 T
Electron Beam Velocity Ratio (α)	1.3
Electron Beam Velocity Spread ($\Delta\alpha$)	2.39 %
Electric Field at Cathode (E_c)	6.5 kV/mm
Electron Beam Radius (R_b)	8.11 mm
Electron Beam Thickness (ΔR_b)	1.24 %

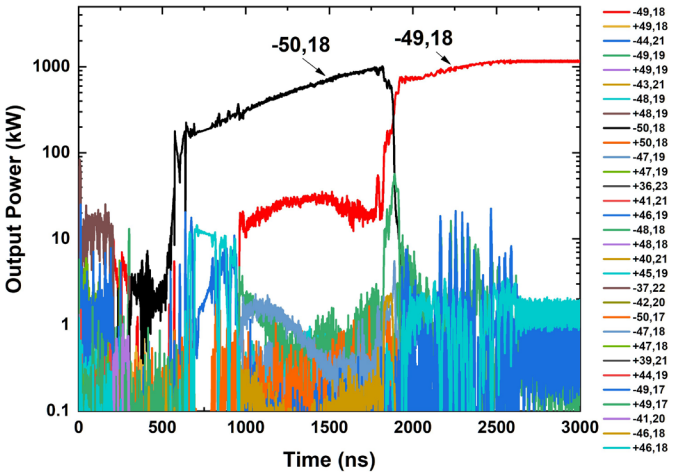

Fig. 7. Output power growth (in logarithmic scale) with time of the desired mode $\mathbf{TE_{49,18}}$ obtained through the KIT SELFT code [20] with 30 competing modes corresponding to linear rise of V_b up to 78 kV whereas R_b = 8.11 mm, α = 1.3, I_b = 45 A, and B_0 = 11.96 T are kept constant.

TABLE VII
THE ELECTRON BEAM PARAMETERS FOR START-UP BEHAVIOR BEFORE THE SPACE-CHARGE NEUTRALIZATION FOR 300-GHZ OPERATION

V_{acc} (kV)	V_m (kV)	I_b (A)	V_b (kV)	α	$\beta_\perp$
78	35.5	45	70.08	1.3	0.37
73	33	43.53	66.01	1.06	0.33
68	31.5	42.01	61.19	1.02	0.32
63	28	40.44	56.95	0.79	0.27
58	25.5	38.8	52.08	0.75	0.25
53	23	37.09	47.26	0.7	0.23

spread ($\Delta\alpha$) for better RF power growth at the desired mode. Further, we have used Baird and Lawson's trade-off expressions [24] to determine the initial dimensions of T-MIG, such as the cathode radius R_c, emitter slant length (L_e), and anode radius (R_a). These calculations are performed using GDS-2018 [18] to achieve high-quality annular electron beam parameters, as stated in Table VI. Using Baird and Lawson's initial approximation results, the proposed T-MIG geometry is optimized further using the particle trajectory code EGUN [19] to generate a hollow electron beam with targeted parameters. The required magnetic field profile should be considered in the EGUN simulations to produce the desired electron beam parameters.

Further several adverse phenomena such as the mirroring effect and potential barriers should be taken care of in the design of a T-MIG under the influence of the magnetic field for the stable operation of the gyrotron. The mirroring effect occurs when the pitch factor is very large. The electrons with low kinetic energy get trapped into the potential barriers. The velocity spread determines the quality of the annular electron beam for efficient energy transfer in between RF wave and electron beam. When the J_e is very low, it is impossible to achieve the minimum velocity spread. Ideally, J_e should be less than 5 A/cm^2 to ensure long operation hours of the MIGs [25]. At the emitting strip of the cathode, the current den- sity can be expressed as $J_e = I_b cos\phi_e / (L_e(2R_e - tan\phi_e L_e))$, where I_b is the electron beam current, R_e is the emitter radius, ϕ_e is the slant angle and L_e is the slant length of the emitter. There are several ways to decrease the current density (J_e), such as decreasing L_e or increasing R_e [25]. The increase in the emitter radius results in an increase in the T-MIG and bore-hole diameter, which would increase the production and maintenance cost of the system. So, a trade-off is required between the diameter of the magnetic bore-hole and the beam quality. The main constraints that should be taken care of for a meticulous operation of the gyrotrons are the accelerating voltage, proper positioning of the annular electron beam for maximum coupling, electron beam current, lower energy spreads (< 5 %), minimum cathode emission density, and maximum perpendicular energy [26]. The optimized electron beam profile is shown in Fig. 6, where the cathode, modulating anode, and accelerating anode are positioned with proper cathode and modulating anode gap aligned along with the equipotential lines. The optimized gun parameters and the simulated results of the designed T-MIG are shown in Table VI.

IV. TIME-DEPENDENT MULTI-MODE SIMULATIONS

Time-dependent multi-mode calculations are performed to confirm the power growth at the desired mode inside the interaction cavity using the KIT SELFT code [20]. Initially,

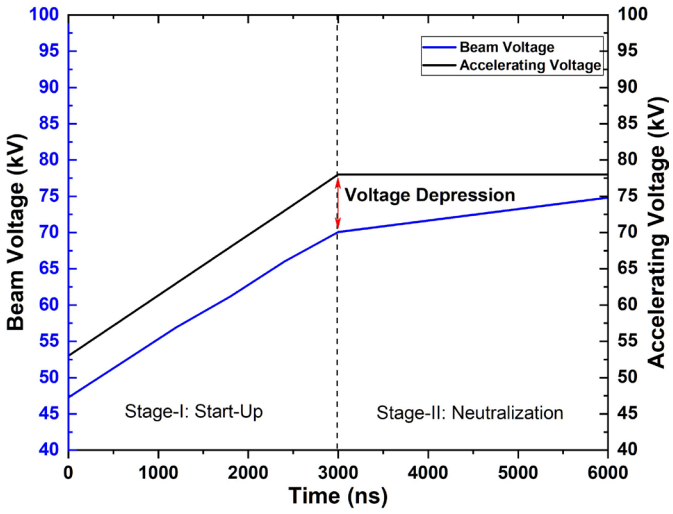

Fig. 8. Variation of V_b with increasing accelerating voltage V_{acc} during diode type start-up.

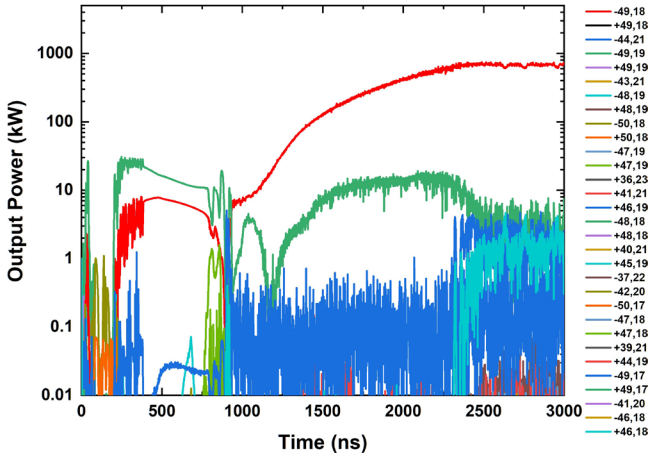

Fig. 9. Output power growth (in logarithmic scale) with time during start-up before space-charge neutralization of the desired mode $\mathbf{TE_{49,18}}$ with R_b = 8.11 mm and 30 competing modes corresponding to linear rise of V_b from 47.26 to 70.08 kV with the electron beam parameters depicted in Table VII.

normalized longitudinal field distribution of the modes are determined from the cold cavity calculations through GDS 2018 [18], whereas the initial amplitude of the field profile of all modes is determined by considering the RF power of the modes as 1.0 W. Time-dependent multi-mode simulations are carried out with the optimized parameters obtained using single-mode self-consistent calculations. The V_b is varied linearly from 53-78 kV, whereas the $\alpha = 1.3$, $I_b = 45$ A, and $B_0 = 11.96$ T at the cavity center are kept constant. In the frequency range of 290 to 310 GHz, all the neighboring modes having Q_d times relative coupling greater than 30% of the operating mode are considered for the time-dependent multi-mode simulations. A total number of 31 modes are considered from the dense mode spectra for the calculations with $R_b = 8.11$ mm. In Fig. 7, initially the critical competing mode $TE_{50,18-}$ dominates, but as time progresses and when V_b reaches to 70 kV, the desired mode $TE_{49,18}$ oscillates and remains stable for the entire period of the simulation with the output power of 1.17 MW. The amplitude of the other neighboring modes remain under the noise level.

Inside the RF interaction cavity, a scant amount of residual gas is always present. Hence due consideration may be made to the lack of perfect vacuum for the megawatt-class gyrotron operation. V_b gets depressed due to the presence of space-charge. However, the high-energy electron beam ionizes the residual gas molecules in the interaction space, and these ions partially neutralize the space-charge and, as a result, V_b increases to a value close to the accelerating voltage V_{acc} [27], [28]. In the neutralization process, the transverse momentum $\gamma\beta_\perp$ remains invariant and hence α reduces significantly [17]. The neutralization process requires hundred milliseconds to few seconds depending upon several parameters such as initial electron beam parameters and background pressure [28]. In these multi-mode calculations, a start-up behavior is carried out with the space-charge neutralization (SCN). Detailed start- up scenarios of two different types (diode and triode) are explained in [22], [29]. In this design, though T-MIG is used to generate the beam parameters, for simplicity in the start-

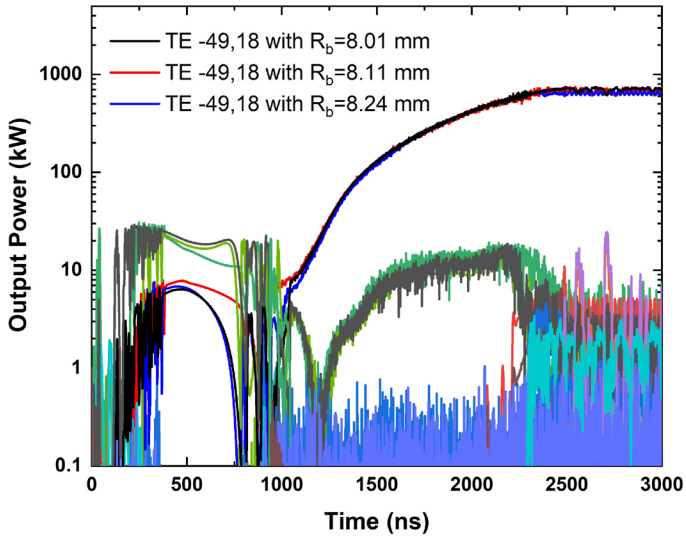

Fig. 10. Effect of electron beam radial spread on the output power growth (in logarithmic scale) at the desired mode $\mathbf{TE_{49,18}}$ of a 300 GHz gyrotron, obtained through the KIT SELFT code [20] with more than 30 competing modes.

up scenario, the diode type start-up is considered. In the diode type start-up as the cathode voltage V_{acc} increases linearly, the simultaneous changes will be reflected in the beam voltage V_b, velocity ratio α and beam current I_b. In the start-up operation, V_b is reduced from the V_{acc} by the amount of voltage depression ΔV_d [30]. The linear rise of the V_b and V_{acc} is plotted in Fig. 8 where two stages are defined, stage-I: Start- up and stage-II: Neutralization. In the start-up operation before the SCN, V_b is raised from 47.26 to 70.08 kV, as stated in Table VII. When V_b reaches 57 kV, the desired mode dominates and remains stable for the entire period with R_b = 8.11 mm. From Fig. 9, it is evident that out of 30 neighboring modes, none dominates in power growth, but as time progresses, the desired mode $TE_{49,18}$ dominates after 1000 ns, and the oscillated power increases up to 720 kW.

The single-mode and multi-mode simulations of the pro

TABLE VIII
THE ELECTRON BEAM PARAMETERS AFTER 60 % SPACE-CHARGE NEUTRALIZATION (SCN) FOR 300 GHZ OPERATION

Scenario	Vb (kV)	Ib (A)	α	β	Pout (kW)		
					8.01 (mm)	8.11 (mm)	8.24 (mm)
Before SCN	70.08	45	1.3	0.37	697	720	665
Partial (60 %) SCN	74.83	45	1.19	0.37	918	924	877

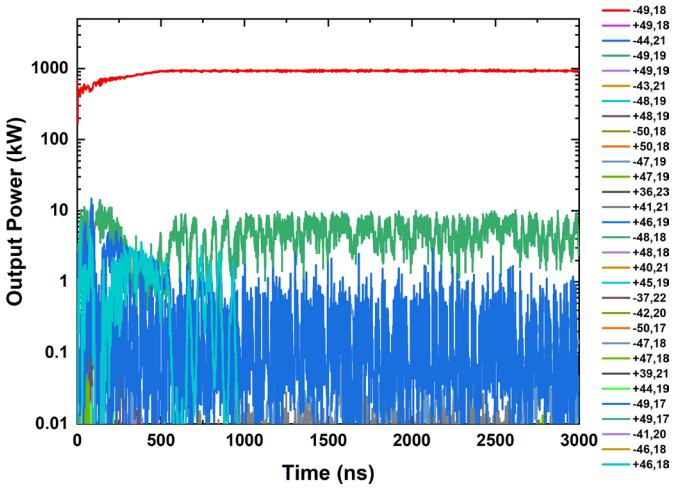

Fig. 11. Output power growth (in logarithmic scale) after space-charge neutralization (60 %) of the desired mode **TE49,18** with R_b = 8.11 mm along with 30 competing modes (with V_b increasing linearly from 70.08 to 74.83 kV over the time period of 3000 ns, corresponding parameters given in Table VIII), obtained using the KIT SELFT code [20].

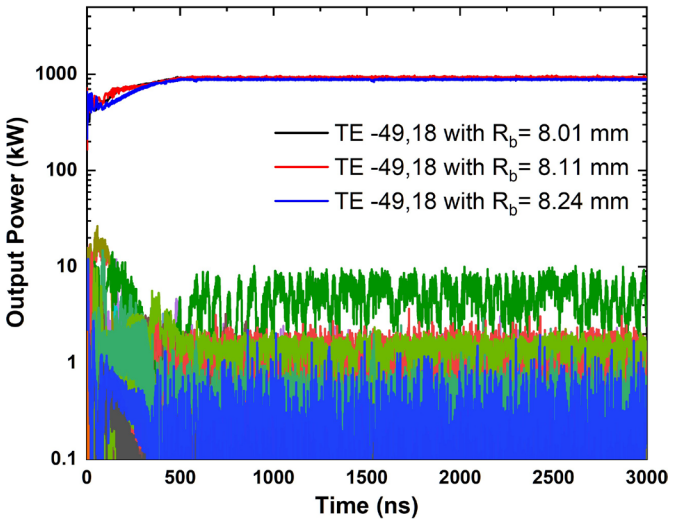

Fig. 12. Effect of electron beam radial spread on the output power growth (in logarithmic scale) after space-charge neutralization (60 %) of the desired mode **TE49,18** along with more than 30 competing modes (with V_b increasing linearly from 70.08 to 74.83 kV over the time period of 3000 ns, corresponding parameters given in Table VIII), obtained using the KIT SELFT code [20].

posed design are carried out with the uniform magnetic field along the interaction cavity. The entire simulation studies are performed with the hollow electron beam that contains 35 beamlets with the azimuthal phase of 53 values for each beamlet and the longitudinal step-size of $\lambda/20$. Each electron in the beamlet generated by the T-MIG may experience different field intensity and may cause radial spread in the electron beam. In the high-frequency regime, the effect of radial spread is significant for the stable operation of high-power gyrotron with highly dense mode spectra. Thus, the effect of electron beam radial spread on the output power at the desired mode is verified with different guiding center radii with more than 30 competing modes, as shown in Fig. 10, where V_b is raised from 47.26 to 70.08 kV. In the time-dependent multi-mode studies, the maximum (8.24 mm) and minimum (8.01 mm) guiding center radii are calculated with respect to the guiding center spread ΔR_b $\lambda/4$. From Fig. 10, it is evident that the output power slightly differs with the radial beam spread. It is noted that 720 kW of output power is obtained with 8.11 mm of beam radius, whereas 697 and 665 kW of power is achieved with 8.01 and 8.24 mm of beam radius, respectively.

Additionally, multi-mode calculations are carried out with more than 30 competing modes to obtain partial (60 %) SCN where V_b is varied from 70.08 to 74.83 kV over the time period of 3000 ns, whereas the velocity ratio (α) and electron beam current (I_b) are varied as per adiabatic approximation, as stated in Table VIII. After the partial space-charge neutralization (60 %) with R_b = 8.11 mm, the power level increases up to 924 kW and remains stable up to 3000 ns, as shown in Fig. 11, whereas α reduces from 1.3 to 1.19. Further, with R_b = 8.01 and 8.24 mm, the output power level increases up to 918 kW and 877 kW, respectively, as shown in Fig. 12. Hence, the study establishes a stable operation of the designed gyrotron at 300 GHz with the desired output power level for the chosen mode TE49,18.

V. CONCLUSION

A conventional-cavity gyrotron with a T-MIG has been designed to deliver RF output power of 1 MW with 31.59 % interaction efficiency at 300 GHz for its potential employment in modern tokamaks such as DEMO especially for ECRH and ECCD of plasmas. Initial mode selection, mode competition, cold cavity design, magnetic coil design, initial design of the T-MIG and single-mode self-consistent computations are carried out using GDS-2018. The T-MIG design has further been optimized using EGUN to generate the annular electron beam with the desired beam parameters to interact with RF waves in the interaction cavity of the gyrotron with the electron beam radius of 8.11 mm, electron beam velocity ratio of 1.3, and electron beam velocity spread of 2.39 %. Further, the time-dependent multi-mode calculations using the KIT SELFT code have been performed to confirm the output power growth at the desired mode dominating over the other competing modes. The realistic assessments such as Glidcop as interaction cavity material, start-up and partial space-charge neutralization calculations with radial beam spread have confirmed the attainability of the desired level of stable output power. The efficiency of such a gyrotron can further be improved by suitably employing one- or two-stage depressed collector system which is not in the purview of the present work. However, we are planning to design an effective output system for such a gyrotron which is the future scope of this work.

REFERENCES

[1] S. Sabchevski, M. Glyavin, S. Mitsudo, Y. Tatematsu, and T. Idehara, "Novel and Emerging Applications of the Gyrotrons Worldwide: Current Status and Prospects," *Journal of Infrared, Millimeter, and Terahertz Waves,* 2021, doi:10.1007/s10762-021-00804-8.

[2] M. V. Kartikeyan, E. Borie, and M. K. A. Thumm, "Gyrotrons-High Power Microwave and Millimeter Wave Technology," *Berlin-Heidelberg, Springer-Verlag, Germany,* 2004.

[3] M. K. A. Thumm, G. G. Denisov, K. Sakamoto and M. Q. Tran, "High-Power Gyrotrons for Electron Cyclotron Heating and Current Drive," *Nucl. Fusion,* vol. 59, No. 073001, 2019.

[4] M. Thumm, "State-of-the-Art of High-Power Gyro-Devices and Free Electron Masers," *J. Infrared Millim. Terahertz Waves,* vol. 41, no. 1, pp. 1–140, 2020, doi:10.1007/s10762-019-00631-y.

[5] A. Kasugai, K. Sakamoto, K. Takahashi, K. Kajiwara, and N. Kobayashi, "Steady-state operation of 170 GHz–1 MW gyrotron for ITER," *Nucl. Fusion,* vol. 48, no. 5, 054009, 2008.

[6] M. Henderson *et al.*, "The targeted heating and current drive applications for the ITER electron cyclotron system," *Physics of Plasmas,* vol. 22, no. 2, p. 021808, 2015, doi:10.1063/1.4908598.

[7] M. Schmid, J. Franck, P. Kalaria, K. A. Avramidis, G. Gantenbein, S. Illy, J. Jelonnek, I.G. Pagonakis, T. Rzesnicki, M. Thumm, "Gy- rotron development at KIT: FULGOR test facility and gyrotron con- cepts for DEMO," *Fusion Eng. Des.,* vol. 96–97, pp. 589–592, 2015, doi:10.1016/j.fusengdes.2015.03.003.

[8] S. Ruess *et al.*, "KIT coaxial gyrotron development: from ITER toward DEMO," *Int. J. Microw. Wirel. T.,* vol. 10, no. 5–6, pp. 547–555, 2018, doi:10.1017/S1759078718000144.

[9] J. Jelonnek *et al.*, "Design considerations for future DEMO gyrotrons: A review on related gyrotron activities within EUROfusion," *Fusion Eng. Des.,* vol. 123, pp. 241–246, 2017, doi:10.1016/j.fusengdes.2017.01.047.

[10] N. Kumar and A. Bera, "RF Behavior of a Coaxial Interaction Structure for 0.24-THz, 2-MW Gyrotron," *IEEE Trans. Electron Devices,* vol. 67, no. 8, pp. 3369-3377, Aug. 2020, doi: 10.1109/TED.2020.3000975.

[11] G. G. Denisov *et al.*, "First experimental tests of powerful 250 GHz gyrotron for future fusion research and collective Thomson scattering diagnostics," *Review of Scientific Instruments,* vol. 89, no. 8, p. 084702, 2018, doi: 10.1063/1.5040242.

[12] T. Kariya *et al.*, "Development of over-MW gyrotrons for fusion at 14 GHz to sub-THz frequencies," *Nucl. Fusion,* vol. 57, no. 6, p. 066001, 2017, doi:10.1088/1741-4326/aa6875.

[13] E. Poli, G. Tardini, H. Zohm, E. Fable, D. Farina, L. Figini, N.B. Marushchenko and L. Porte, "Electron-cyclotron-current-drive efficiency in DEMO plasmas," *Nucl. Fusion,* vol. 53, 013011, 2013.

[14] M. Thumm *et al.*, "Towards a 0.24-THz, 1-to-2-MW-class gyrotron for DEMO," *Terahertz Science and Technology,* vol. 8, no. 3, 85-100, 2015.

[15] P. C. Kalaria, K. A. Avramidis, J. Franck, G. Gantenbein, S. Illy, I. G. Pagonakis, M. Thumm, and J. Jelonnek, "Systematic Cavity Design Approach for a Multi-Frequency Gyrotron for DEMO and Study of its RF Behavior," *Phys. Plasmas,* vol. 23, no. 9, p. 092503, 2016, doi:10.1063/1.4962238.

[16] Q. Liu *et al.*, "Thermoanalysis and Its Effect on the Multimode Beam-Wave Interaction for a 0.24-THz, Megawatt-Class Gyrotron," *IEEE Trans. Electron Devices,* vol. 65, no. 2, pp. 704-709, Feb. 2018, doi: 10.1109/TED.2017.2783927.

[17] S. Yuvaraj, M. V. Kartikeyan and M. K. Thumm, "Design Studies of a 3-MW, Multifrequency (170/204/236 GHz) DEMO Class Triangular Corrugated Coaxial Cavity Gyrotron," *IEEE Trans. Electron Devices,* vol. 66, no. 1, pp. 702–708, 2019, doi: 10.1109/TED.2018.2876870.

[18] S. Yuvaraj, G. S. Baghel, S. Singh, and M. V. Kartikeyan, "Gyrotron Design Suite (GDS-2018)," *Private Communication*, Dec. 2018.

[19] W.B. Herrmannsfeld, "EGUN: An electron optics and gun design program," in *Stanford Linear Accelerator Center, Menlo Park, CA (USA),* 1988, doi: 10.2172/6711732.

[20] S. Kern, "Numerische Simulation der Gyrotron-Wechselwirkung in Koaxialen Resonatoren," *Karlsruhe Inst. Technol., Karlsruhe, Germany, Sci. Rep. 5837,* Nov. 1996.

[21] J. Franck, K. Avramidis, G. Gantenbein, S. Illy, J. Jin, M. Thumm and J. Jelonnek, "A generic mode selection strategy for high-order mode gyrotrons operating at multiple frequencies," in *Nucl. Fusion,* vol. 55, no. 1, Art. no. 013005, Jan. 2015, doi:10.1088/0029-5515/55/1/013005.

[22] P. C. Kalaria, "Feasibility and Operational Limits for a 236 GHz Hollow-Cavity Gyrotron for DEMO,"*Scientific Publishing, KIT,* ISBN: 978-3-7315-0717-8, 2017.

[23] A. R. Choudhury, "Investigations of After Cavity Interaction in Gyrotrons Including the Effect of Non-uniform Magnetic Field," in *PhD thesis, KIT, Karlsruhe,* 2014.

[24] J. M. Baird and W. Lawson, "Magnetron injection gun (MIG) design for gyrotron applications," in *Int. J. Electron.,* vol. 61, no. 6, pp. 969–984, Jun. 1986. doi.org/10.1080/00207218608920932.

[25] M. H. Beringer, "Design Studies towards a 4 MW, 170 GHz Coaxial-Cavity Gyrotron," in *KIT Scientific Publishing,* 2011, ISSN: 2192-2764.

[26] Y. Yamaguchia, Y. Tatematsu, T. Saito, R. Ikeda, J. C. Mudiganti, I.Ogawa, and T. Idehara, "Formation of a laminar electron flow for 300 GHz high-power pulsed gyrotron," in *Phys. Plasmas,* vol. 19, pp. 113113-1–113113-6, Nov. 2012, doi: 10.1063/1.4768959.

[27] A. P. Fokin, M. Y. Glyavin, and G. S. Nusinovich, "Effect of ion compensation of the beam space charge on gyrotron operation," *Physics of Plasmas,* vol. 22, no. 4, p. 043119, 2015, doi:10.1063/1.4918947.

[28] A. Schlaich *et al.*, "Frequency-Based Investigation of Charge Neutralization Processes and Thermal Cavity Expansion in Gyrotrons," *J. Infrared Millim. Terahertz Waves,* vol. 36, no. 9, pp. 797–818, 2015, doi:10.1007/s10762-015-0177-1.

[29] G. S. Nusinovich *et al.*, "Startup scenarios in high-power gyrotrons," in *IEEE Trans. Electron Devices,* vol. 32, no. 3, pp. 841-852, June 2004, doi: 10.1109/TPS.2004.828854.

[30] E. Borie and G. Gantenbein, "Self consistent theory for gyrotrons including effect of voltage depression," in *J. Infrared Millim. Terahertz Waves,* vol.12, no. 2, pp.65–78, 1991.